PHOTONICS Research

# Actively controllable terahertz switches with graphene-based nongroove gratings

Linbao Luo,[1] Kuiyuan Wang,[1] Caiwang Ge,[1] Kai Guo,[2] Fei Shen,[2] Zhiping Yin,[1,2] and Zhongyi Guo[2,*]

[1]School of Electronic Science and Applied Physics, Hefei University of Technology, Hefei 230009, China
[2]School of Computer and Information, Hefei University of Technology, Hefei 230009, China
*Corresponding author: guozhongyi@hfut.edu.cn

Received 3 July 2017; revised 26 August 2017; accepted 3 September 2017; posted 18 September 2017 (Doc. ID 301553); published 26 October 2017

**We systematically investigated the tunable dynamic characteristics of a broadband surface plasmon polariton (SPP) wave on a silicon-graded grating structure in the range of 10–40 THz with the aid of single-layer graphene. The theoretical and numerical simulated results demonstrate that the SPPs at different frequencies within a broadband range can be trapped at different positions on the graphene surface, which can be used as a broadband spectrometer and optical switch. Meanwhile, the group velocity of the SPPs can be modulated to be several hundred times smaller than light velocity in vacuum. Based on the theoretical analyses, we have predicted the trapping positions and corresponding group velocities of the SPP waves with different frequencies. By appropriately tuning the gate voltages, the trapped SPP waves can be released to propagate along the surface of graphene or out of the graded grating zone. Thus, we have also investigated the switching characteristics of the slow light system, where the optical switching can be controlled as an "off" or "on" mode by actively adjusting the gate voltage. The slow light system offers advantages, including broadband operation, ultracompact footprint, and tunable ability simultaneously, which holds great promise for applications in optical switches.** 

***OCIS codes:*** (050.2770) Gratings; (200.6715) Switching; (230.7370) Waveguides; (240.6680) Surface plasmons.

https://doi.org/10.1364/PRJ.5.000604

## 1. INTRODUCTION

Surface plasmon polaritons (SPPs) are electromagnetic (EM) waves coherently coupled to electron oscillations that present the confined EM field at the corresponding metal interface, which can efficiently slow down the light and realize light manipulation in the nanoscale [1]. Noble metals, like silver and gold, are typically regarded as the dominant materials for supporting SPPs at the visible and near-infrared range. Even in the terahertz (THz) range, SPP-based slow light systems can also be realized by using different noble metal nanostructures, such as a flat metal stripe or metal-graded period grating [2,3]. Such SPP-based systems have the advantages of overcoming the diffraction limit of light and providing the possibility of the miniaturization of slow light devices [4]. However, in the THz range, SPPs have weak confinement and high loss on the metal surface, so the noble metals are unsuitable in this waveband. In addition, the large electronic density of states in metals also restricts the possibility of dynamically tuning their permittivity in active plasmonic devices. Current THz active plasmonic devices can be usually realized with the assistance of another active material, including transparent conducting oxides, superconductors, and graphene.

Graphene, a 2D material of carbon atoms arranged in a honeycomb lattice, whose optical response is characterized by surface conductivity, behaves like the thin metal films with negative permittivity via external tunability, such as the electric field, chemical doping, and gate voltage at the THz range [5–7]. These unique optical features have made graphene a promising candidate for novel nanophotonic devices, such as superlens, optical hyperlens, and SPP waveguides [6,8,9]. The propagation of SPP waves along the graphene sheet have large wave vectors as well as extremely high field confinement, which enables us to build potential optical devices with dimensions significantly below the diffraction limit. In addition, the large manipulating characteristics of graphene's permittivity may enable freedom to control the devices' performances during operation. It is therefore inferred that graphene plasmonics (GPs) are promising in THz to the mid-infrared region (MIR), where there are various significant applications of slow light systems. In fact, the application of GP-based THz slow light systems has been extensively investigated. For example, Chen *et al.* first reported the GPs "rainbow trapping" by linearly increasing the grooves' width of silicon grating [10]. Then Lu *et al.* proposed another GPs "rainbow trapping" structure based on a graded

depth of silicon-grating to trap the generated SPPs of different frequencies at different positions [11]. Nasari and Abrishamian took advantage of the strong EM field of GPs to design a tunable THz Bragg reflector by using the Kerr nonlinear medium [12]. Recently, Shi *et al.* designed a tunable band-stop filter based on GPs with periodically modulated chemical potentials [13]. However, there is little work focusing on the THz plasmonic switch. The THz plasmonic switch is actually an important component in modern telecommunication systems. The GPs offers the potential building blocks for developing ultracompact, high-performance, and actively tunable THz switch devices. Recently, a deep-wavelength THz plasmonic waveguide has been proposed by means of a graphene-metal structure, performing as a THz switch or an AND/OR logic gate [14], which is still difficult for practical implementation because of the complicated structures and suffering from high loss in the metal.

In this paper, we propose a novel THz switch based on a graphene monolayer covered nongroove silicon graded-width grating, in which the graphene and silicon are separated by polymethylmethacrylate (PMMA) as an interlayer, and the optical properties of graphene can be tuned via an external gate voltage. We theoretically and numerically demonstrate that the SPPs at different frequencies within a broadband region can be trapped at different positions on the graphene surface. The group velocity of the generated SPPs can also be reduced several hundred times than light velocity in vacuum. The trapping positions of the generated SPPs with given frequencies can be accurately predicted; therefore, our proposed system can function as a broadband spectrometer. Furthermore, the release of the trapped waves can be realized by actively tuning the gate voltage. Once a certain threshold voltage for a given trapped wave is reached, the wave will finally be out of the graded grating zone, which can function as an optical switch in broadband by actively adjusting the gate voltage. The proposed structure would also find broad applications in other fields, such as optical storage, signal processing, nonlinear optical enhancement, and so on.

## 2. RESULTS AND DISCUSSION

### A. Basic Model and Analytical Theory

We first consider a uniform silicon-grating structure, which consists of a graphene monolayer on a silicon-grating substrate with a dielectric layer of PMMA, as schematically shown in Fig. 1. A gate voltage is applied between the graphene sheet and substrate to turn the Fermi energy of graphene by the electric-field effect [15]. The distribution of the electric field is periodical due to the periodical distribution of the depths of $d_1$ and $d_2$, which result in the periodical distributions of the chemical potential and the conductivity in the graphene layer. The monolayer graphene can be characterized by a complex-valued surface conductivity $\sigma_g$, which can be modeled following the Kubo formula [16]. The frequency-dependent surface conductivity can be expressed as a sum of two terms:$\sigma_g = \sigma_{\text{intra}} + \sigma_{\text{inter}}$. The first term corresponding to the intraband electron-photon scattering can be described as

$$\sigma_{\text{intra}} = i\frac{e^2 K_B T}{\pi^2(\omega + i\tau^{-1})}\left\{\frac{\mu_c}{K_B T} + 2\ln\left[\exp\left(-\frac{\mu_c}{K_B T}\right) + 1\right]\right\}. \quad (1)$$

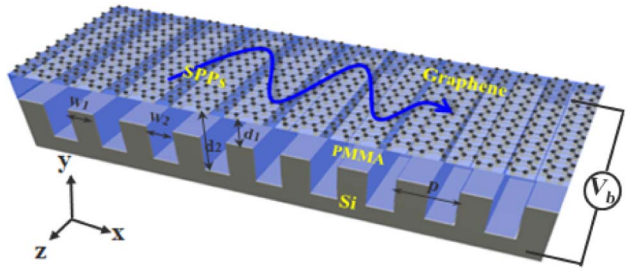


**Fig. 1.** Schematic of a uniform graphene-based grating structure: a graphene monolayer on a uniform silicon grating structure with PMMA as the interlayer. $p$ is the grating period, $w_1$ and $w_2$ denote the widths of nongroove parts and groove parts of the grating, $w_2$ is fixed at 30 nm in our work, and $d_1$ and $d_2$ are the depths of graphene sheet to nongroove and groove parts, respectively.

And the second term corresponding to the interband transition contribution, for $\hbar\omega \gg K_B T$ and $|\mu_c| \gg K_B T$, can be described as

$$\sigma_{\text{inter}} = i\frac{e^2}{4\pi\hbar^2}\ln\left[\frac{2|\mu_c| - \hbar(\omega + i\tau^{-1})}{2|\mu_c| + \hbar(\omega + i\tau^{-1})}\right], \quad (2)$$

where $e$ is the electron charge, $K_B$ is the Boltzmann's constant, $T$ is the temperature, $\mu_c$ is the chemical potential, $\omega$ is the angular frequency, $\hbar$ is the reduced Planck's constant, and $\tau$ stands for the momentum relaxation time due to charge carrier scattering. In the MIR, the surface conductivity of graphene can be simplified into the Drude-like form [6]. In graphene, $\tau$ depends on the carrier mobility $\mu$ and can be expressed as $\tau = \mu\mu_c/(ev_f^2)$, and the chemical potential can be expressed as $\mu_c = \hbar v_f(\pi n_s)^{1/2}$. Here, the Fermi velocity $v_f$ is set as $10^6$ m/s, the carrier mobility of graphene μ is assumed as $40,000\ \text{cm}^2 \cdot \text{V}^{-1} \cdot \text{s}^{-1}$ at $T = 300$ K [17]. In particular, the doping level of graphene $n_s$ shows a linear dependence on the external gate voltage described as $n_s = \varepsilon_p\varepsilon_0 V_b/(eh)$ [18]. The $\varepsilon_p$ and $V_b$ are the relativity permittivity of the dielectric layer of PMMA and external voltage, respectively.

In the simulations, the proposed graphene-based structures are simulated by using a home-made program based on the finite-element method (FEM). Five-layer meshes are employed to denote the graphene layer, while nonuniform meshes with a maximum element size of 500 nm are adopted to represent the other regions besides graphene. The surface plasmonic wave is excited by a surface current from the left side. Both scattering boundary condition and perfectly matched layers have been used to absorb any reflected and transmitted fields. The graphene monolayer is treated as an ultrathin film layer with a thickness of $\Delta = 1$ nm [19]. The relative permittivity of graphene can be equivalent as [6]

$$\varepsilon_g = 1 + \frac{i\sigma_g}{\omega\varepsilon_0\Delta}. \quad (3)$$

Because SPPs are highly confined on the graphene surface, the influence of Si substrate on the SPP dispersion can be neglected in our GPs structures [11]. By matching the boundary conditions for the air-graphene-PMMA spacer system, the dispersion relation of SPP modes in graphene can be derived from Maxwell's equations [20]:

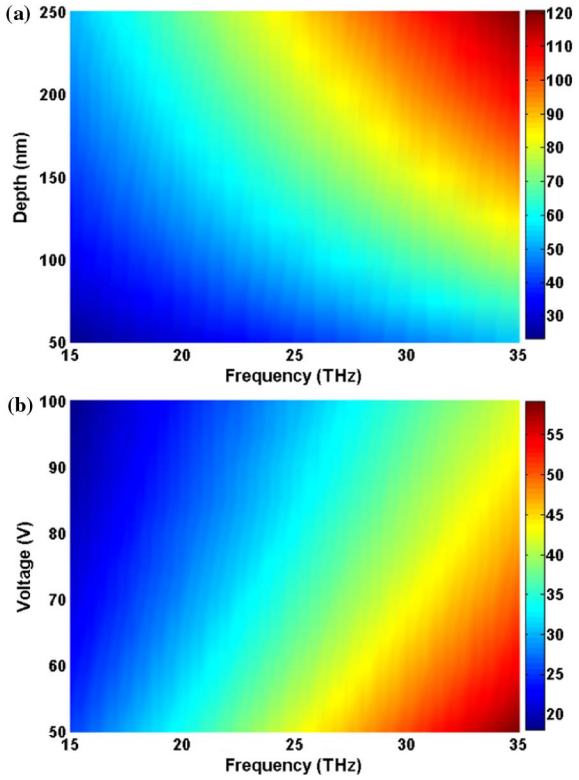


**Fig. 2.** Real parts of the effective refractive index (neff) of SPP modes supported by the graphene monolayer, (a) as the function of frequency and the PMMA spacer depth $d = d_1 = d_2$ with a constant gate voltage of $V_b = 60$ V, and (b) as the function of frequency and the influence of the gate voltage $V_b$ with constant PMMA spacer ($d = d_1 = d_2 = 50$ nm).

$$\frac{\varepsilon_c}{k_0\sqrt{n_{\text{eff}}^2 - \varepsilon_c}} + \frac{\varepsilon_p}{k_0\sqrt{n_{\text{eff}}^2 - \varepsilon_p}} + \frac{i\sigma_g}{\omega\varepsilon_0} = 0, \tag{4}$$

where $k_0 = 2\pi/\lambda$ is the free-space wave vector of light, $\lambda$ is the incident wavelength in vacuum, $n_{\text{eff}}$ is the effective refractive index of SPP mode, $\varepsilon_p$ is the relative permittivity of PMMA, $\varepsilon_c$ denotes the relative permittivity of air, and $\varepsilon_0$ is the permittivity of air. Here, we set $\varepsilon_c = 1$, $\varepsilon_p = 2.25$, respectively [21]. According to Eq. (4), the surface conductivity of graphene determines the $n_{\text{eff}}$ of the SPP mode, which is sensitive to the depth ($d$) and gate voltage $V_b$. As show in Figs. 2(a) and 2(b), for a nongrating structure ($d = d_1 = d_2 = 50$ nm), the real part of effective refractive index Re($n_{\text{eff}}$) as a function of $d$ and $V_b$ can be obtained by solving Eqs. (1)–(4). The real parts of $n_{\text{eff}}$ increase significantly with increasing spacer depth of $d$ and show a pronounced decrease with increasing gate voltage of $V_b$. Therefore, for a uniform graphene-based silicon-grating structure, the different depths and gate voltages can result in different effective refractive index.

### B. Uniform Grating Structure

For a uniform graphene-based silicon-grating structure (Fig. 1), the dispersion relation can be calculated by the characteristic equation [22]:

$$\cos(Kp) = \frac{(n_{\text{eff},1} + n_{\text{eff},2})}{4n_{\text{eff},1}n_{\text{eff},2}}\cos(\varphi_1 + \varphi_2) - \frac{(n_{\text{eff},1} - n_{\text{eff},2})}{4n_{\text{eff},1}n_{\text{eff},2}}\cos(\varphi_1 - \varphi_2), \tag{5}$$

where $K$ is the Bloch wave number of the SPPs in the direction along the propagating direction, $p = w_1 + w_2$ is the period of the grating, $\varphi_1 = k_0 n_{\text{eff},1} w_1$ and $\varphi_2 = k_0 n_{\text{eff},2} w_2$ represent the phases of the graphene zones with PMMA depth of $d_1$ (nongroove parts) and $d_2$ (groove parts), respectively.

As shown in Fig. 3(a), the dispersion curves of SPP modes in the uniform grating with $w_2 = 30$ nm (groove parts) and $V_b = 60$ V but different $w_1$ (nongroove parts) are calculated by solving Eq. (5). It can be seen that the cutoff frequency demonstrates a visible redshift characteristics with increasing the nongroove parts' width $w_1$. At approaching cutoff frequency, the SPP mode dispersion is flat compared with that of the light (straight line), which implies that the group velocity ($v_g = d_\omega/d_k$) of the SPP mode significantly slows down [21]. Therefore, based on this theory, a slow-light waveguide can be realized. The slow-down factor ($S$), which can describe how many times light has been slowed, is defined as $S = c/v_g$, where the group velocity $v_g$ is obtained from the slope of

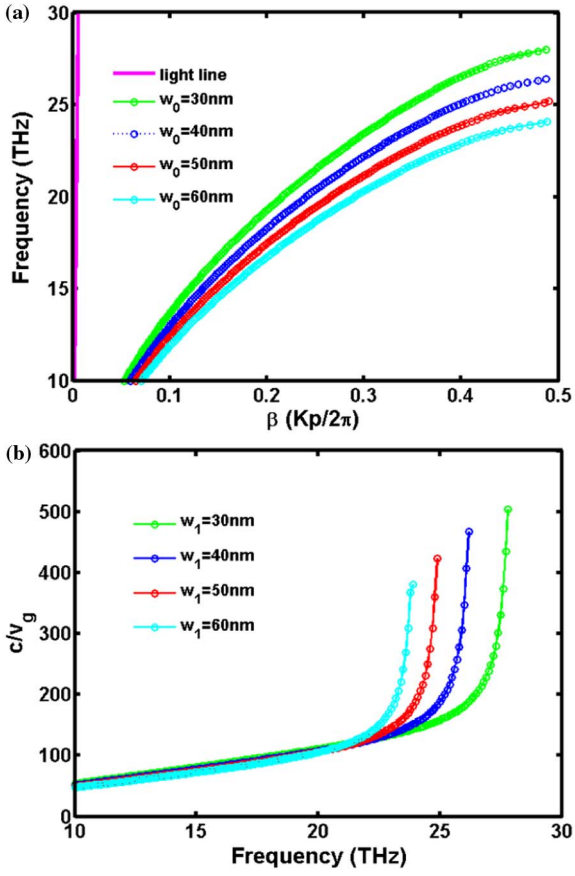


**Fig. 3.** (a) Dispersion curves for different nongroove parts' widths in the graphene-based uniform grating structure. (b) Dependence of slow-down factor $S$ on the excitation frequencies for different nongroove widths. In the calculations, $d_1 = 50$ nm, $d_2 = 250$ nm, $w_2 = 30$ nm, $V_b = 60$ V.

the tangent of a dispersion curve at a given point [23]. Figure 3(b) shows the slow-down factor $S$ as a function of light frequency for different $w_1$, which reveals that the $S$ at the asymptotic cutoff frequency can reach to its maximum value and can significantly be decreased with increasing the $w_1$. It can be seen that the $v_g$ of SPP mode can be reduced to several hundred times than light velocity in vacuum, which could be used for implementing practical slow-light applications. However, the uniform grating structure (with a fixed groove and nongroove widths) can only slow down the group velocity of SPP mode within a rather narrow bandwidth near the cutoff frequency, which hinders further improvement of slow-light capacity.

### C. Graded Grating Structure

In Fig. 3(b), we can find that the most efficient reduction of the group velocity in the graphene-based grating structure occurs when the SPP frequency approaches to the cutoff value of a given nongroove width $w_1$. The $w_1$ for the most pronounced slowdown factor increases with increasing the operating wavelength. Therefore, to broaden the spectral region where light signal can be slowed down, a graphene-based graded grating structure is proposed, as illustrated in Fig. 4. The graded grating is achieved by linearly increasing the width of nongroove parts, $w_1$, along the $x$ direction, while keeping the width of groove parts, $w_2$, as a constant. Here, the nongroove width $w_1$ is chosen to gradually increase from 30 to 65 nm by a fixed step of $\Delta = 1$ nm. The total length of the graded grating structure is only 2760 nm and the grade ($\Delta = 1$ nm) is small enough, which meet the adiabatic condition ($\delta = \partial k^{-1}/\partial x \approx \frac{1/k_1 - 1/k_2}{p} \ll 1$, where $k_1$ and $k_2$ are the wavenumbers in the adjacent grating units, and $p$ is the period of the grating) and ensure that the stop-band edge of the graded grating changes slowly with the position along the structure as the nongroove widths increase [24].

As shown in Fig. 5(a), the theoretical results show that the SPP modes with different incident wavelengths can be trapped at different positions along the graphene monolayer, associated with the corresponding nongroove width $w_1$. A broadband of 5.6 THz wave within a range of 28.6–34.2 THz can be dramatically slowed down in the designed grating system. The theoretical prediction above can be validated by 2D FEM simulations, as shown in the dash–dot lines in Fig. 5(a). The light excitation in the MIR and a TM polarized SPP mode will propagate along the graphene monolayer. For example, the waves with the wavelengths of 9, 9.5, and 10 μm are trapped at $x = 280$, 975, and 1855 nm, corresponding to the nongroove width of $w_1 = 34$, 44, and 55 nm. Figure 5(b) illustrates the corresponding electric field intensity ($|E_y|^2$) distribution in the $x$–$y$ plane of the structure for incident wavelengths of 9, 9.5, 10 μm, and the incident waves are trapped at different positions along the graphene waveguide, respectively, which result in the so-called "trapped rainbow" and can be used for the storage of light.

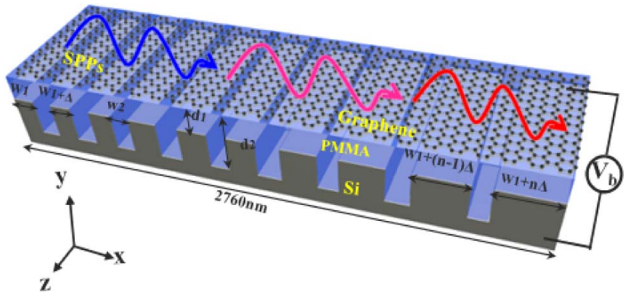


**Fig. 4.** Schematic illustration of the graphene-based graded grating structure. Here, $d_1 = 50$ nm, $d_2 = 250$ nm, $w_2 = 30$ nm, and $V_b = 60$ V. The nongroove width increases linearly from 30 to 65 nm with a step of $\Delta = 1$ nm; in our simulations, the width of the whole structure along the $x$ axis is 2760 nm.

We can clearly observe that the electric field intensity reaches its maximum value near the corresponding cutoff position, associated with the nongroove width of $w_1$, but shows a gradual reduction as the increase of the excitation wavelength [Fig. 5(c)]. As shown in Figs. 5(a) and 5(b), we can know that the propagation distance increases with increasing the excitation wavelength, so the absorption loss in graphene also increases as the propagation of the SPP mode along the graphene surface. In addition, the group velocity of SPP mode can also be effectively reduced in the graphene-based graded grating structure. Figure 5(d) reveals the slow-down factor as a function of the trapping position of the SPP mode for the incident wavelengths of 9, 9.5, and 10 μm, accordingly. We can find that the slow-down factor strongly depends on the nongroove width at a given excitation wavelength. The most efficient reduction of the group velocity in the structure presented here occurs when the nongroove width $w_1$ approaches the cutoff value of a given frequency. For example, the slow-down factor up to 375 at $x = 1855$ nm corresponding to the nongroove width $w_1 = 55$ nm when the excitation wavelength is 10 μm. In a word, we can clearly predict that the incident wave with different frequencies will stop at different positions along the graphene-based graded grating system, from which they will be separated to different positions. Therefore, such a graphene-based slow-down system can be used to disperse different frequency components of the incoming THz signals and function as a broadband spectrometer.

### D. Active Optical Switching Performance

The next question is how to release the trapped waves at different positions along the graded grating. It has been demonstrated that trapped waves in the previous metal-based plasmonic rainbow trapping systems can be released by capping the metal grating with a dielectric material and temperature-tune the refractive index of the material filling the grooves via the thermo-optic effect [25]. However, a complete release within a wide bandwidth is still challenging due to the comparatively small refractive variation induced by the thermo-optic materials. In addition, the temperature change may also affect the optical performance of the device. As discussed in the previous section [Figs. 1(a) and 1(b)], we can know that the spacer depth and gate voltage can modulate the dispersion relation of SPP modes. Therefore, to our graphene-based graded grating structure above, one approach might be the use of a piezoelectric material to replace the PMMA as the dielectric interlayer, whose thickness properties could be temporally modulated by an external electric field [26]. Alternatively, we could also employ the other more feasible way to control the graphene's surface conductivity to tune the dispersion relation of SPP modes by adjusting the external gate voltage.

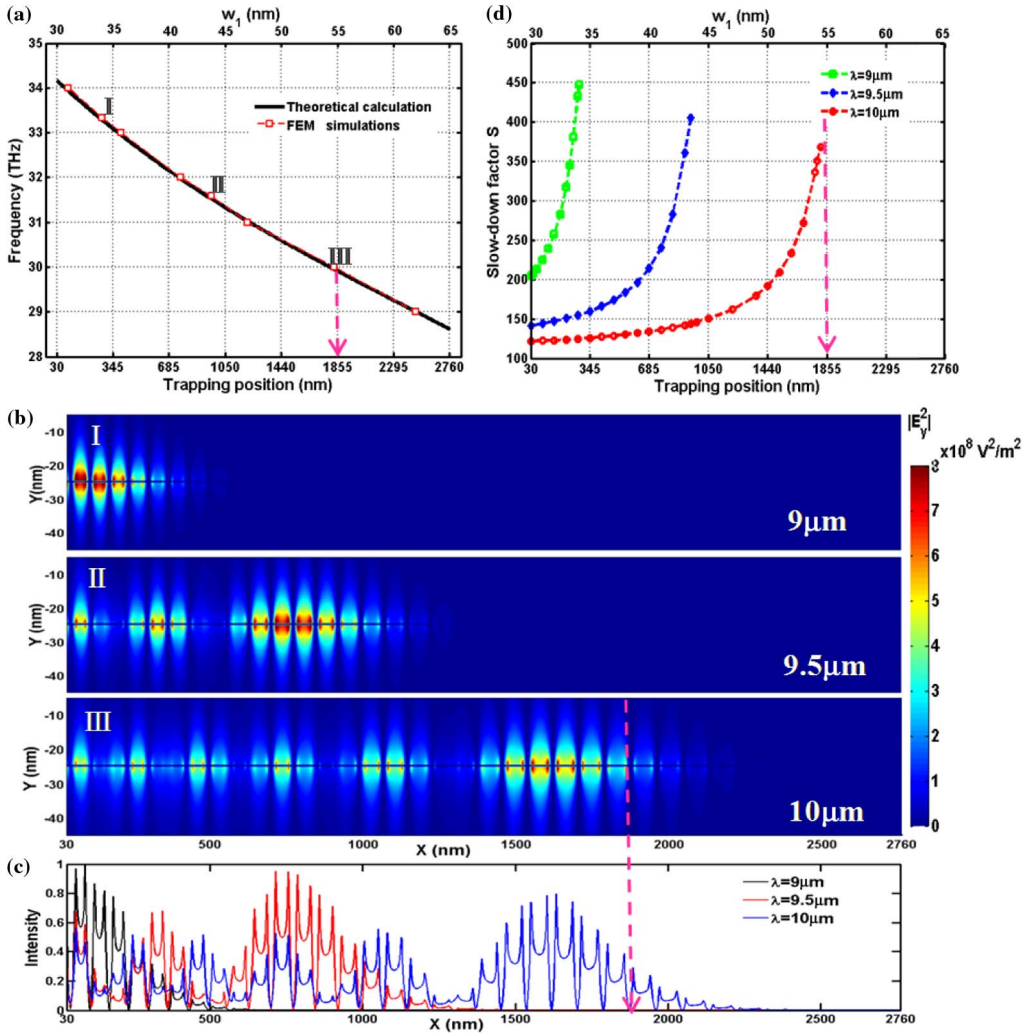


**Fig. 5.** (a) Trapping position as a function of cutoff frequency. (b) Electric field distributions of $|E_y|^2$ in the $x$–$y$ plane of the graphene graded grating structure in Fig. 4 for incident wavelengths of 9, 9.5, and 10 μm, respectively. (c) Corresponding normalized field intensities distribution 2 nm above the graphene surface. (d) The slow-down factor $S$ as a function of trapping position for different operating wavelength.

As shown in Fig. 6(a), the value of the cutoff frequency for the SPP mode undergoes a blueshift as $V_b$ increases for a given $w_1$. For example, the cutoff frequency for $w_1 = 30$ nm with $V_b = 60$ V is 34.4 THz, which shifts to 36.9 THz with $V_b = 80$ V. Namely, the trapped SPPs located at the corresponding position will move to the other position with adjusting the external gate voltage. If the $V_b$ is big enough, the trapped waves will be released and outputted from the edge of the graphene-based waveguide [see Fig. 6(b)]. As illustrated in Fig. 6(b), the dotted line shows the trapping positions of 30 THz shifts from 306 to 1855 nm along the $x$ axis when the gate voltage increased from 40 to 60 V. When the $V_b$ further increased to 80 V, the trapped wave will be released from the graphene waveguide. Thus, the trapped waves are released as the gate voltage increases. Figure 6(c) illustrates the corresponding electric field intensity ($|E_y|^2$) distributions for incident frequency of 30 THz ($\lambda = 10$ μm) at $V_b = 40$, 60, and 80 V, which agree well with the corresponding results of the above theoretical prediction.

In addition, it should be noted that the trapped frequency span is from 24.8 to 30.8 THz at $V_b = 40$ V, while the span will shift to 27.2–34 THz by increasing the gate voltage to 80 V. In other words, this trapped frequency span can be actively tuned by changing the gate voltage between the silicon substrate and the graphene sheet. Thus, the trapping band can be flexibly broadened for a given graphene-based graded grating structure. Once a certain threshold voltage for a given trapped wave is reached, the wave will finally be able to propagate along the graphene waveguide and out of the graded grating zone, which can function as a tunable broadband optical switching. The optical switching can actively control "off" or "on" by properly adjusting the gate voltage. If we want to realize the optical switching characteristics for our designed system, there will be a critical voltage for different wavelengths of incident waves, which has been calculated and plotted as a function of frequency, as shown in Fig. 7. The critical voltage increases with the frequency of the optical signal propagated in the graphene-based optical waveguide. In a word, the structure provides a flexibly broadband slow SPP waveguide to trap and control the light signals in the nanoscale domain, offering potential applications in on-chip light localization, broadband spectrometer, and optical switching.

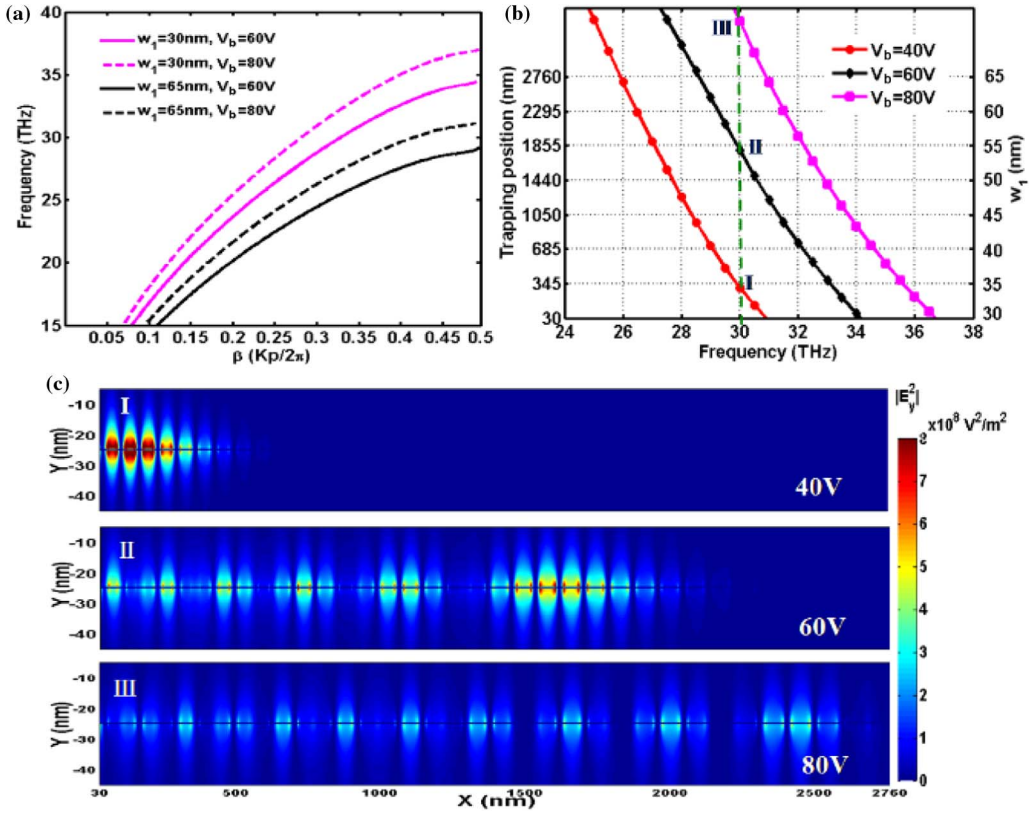


**Fig. 6.** (a) Dispersion curves for $w_1 = 30$ nm and $w_1 = 65$ nm with different gate voltages ($V_b = 60$ V and $V_b = 80$ V). (b) Trapping position as a function of frequency for different gate voltages. (c) Electric field distributions of $|E_y|^2$ in the $x$–$y$ plane of the structure in Fig. 4 for 10 μm of $V_b = 40$, 60, and 80 V, respective.

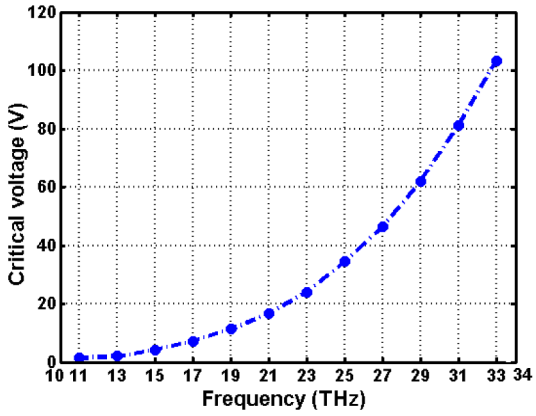


**Fig. 7.** Theoretical critical gate voltages needed to turn on the optical switching as a function of frequency at the position $x = 2760$ nm (output position).

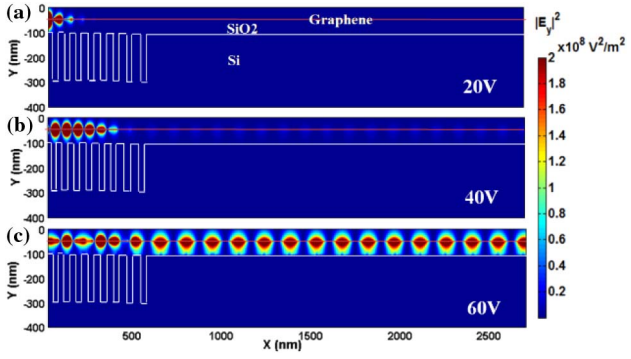


**Fig. 8.** Electric field distributions of $|E_y|^2$ in the $x$–$y$ plane of the modified structure for 10 μm at $V_b = 40$, 60, and 80 V, respectively. White lines mark the material boundaries of the modified structure. The nongroove width increases linearly from 30 to 37 nm with a step of $\Delta = 1$ nm, and the groove width is fixed at 30 nm.

It should be noted that the electric field intensity ($|E_y|^2$) of the SPP mode in Fig. 6 is gradually weakening with increasing the propagation distance. This attenuation can be contributed to the inherent materials absorption, scattering loss, and the coupling loss (due to the mode momentum mismatching) during the longer propagation in the graded grating system. In order to enhance the transmission efficiency of the switching while keeping the characteristic of dynamic adjustment, we have designed a new switching structure consisting of a graded grating (input block) to actively control light and a monolayer graphene waveguide (output block) as an extension to the input block to conduct the propagation wave, respectively, as shown by the white lines in Fig. 8. The nongroove width of the input block increases linearly from 30 to 37 nm with a step of $\Delta = 1$ nm (the groove width is fixed at 30 nm), and the corresponding critical voltage is 45 V. Figure 8(a) shows the field

distribution when the graphene layer is biased by 20 V and incident frequency is 30 THz ($\lambda = 10$ μm), and we can observe that the SPP wave stopped on the front end of the input block, and almost no light can reach to the out block due to the bias voltage being much less than the corresponding critical voltage. When the bias voltage is close to but less than the critical voltage (e.g., 40 V), only little energy can be derived from the input block, which will stop at one certain position in the input block, as shown in Fig. 8(b). And once the bias voltage reaches to and becomes greater than the critical voltage (e.g., 60 V), the switching will be opened; meanwhile, the transmission efficiency is high, which can be confirmed by the corresponding field distribution shown in Fig. 8(c). Furthermore, as depicted in the Figs. 5 and 6, we can know that the switching also has a wide optical bandwidth by applying an appropriate gate voltage. Without changing any design parameters, as long as ascertaining the corresponding critical voltage, one can obtain a wide range of operating wavelengths and a flexible control of transmission efficiency by appropriately tuning the bias voltage, which holds great promise for application in future dynamic switching devices.

### E. Discussion

In fact, with the development of the THz optoelectronic integrated circuits, THz devices have attracted significant attention. Among them, the THz switch is of particular interest because it is a dispensable element for information processing at THz communication and surveillance. In our designed graphene-based-graded grating system, the applied gate voltages can be employed to efficiently tune the trapping positions and group velocity of the trapped SPPs THz. The designed graphene-based graded grating system can also be used as a broadband spectrometer very well. The switching characteristics of the slow light system have been investigated, where the optical switching can be controlled as "off" or "on" modes by actively adjusting the gate voltage.

In comparison with silicon photonic crystal [27], our proposed structure avoids the difficulty of large-scale fabrication and broadens the bandwidth due to the graded structure. In addition, we design the structure with all low-loss materials rather than metal to increase the conversion efficiency [28]. Moreover, we do not have to simultaneously apply different voltages at the central and outer pads, which is a great practical advantage [29,30].

Overall, our graded grating-graphene systems have realized the broadband, miniaturization, tunability, and low-losses characteristics by using graded graphene-based grating and appropriate gate voltage. With the fast development of nanotechniques, such as nanolaser [31], lithography, etc., this approach holds great promise for application in future dynamic switching devices.

## 3. CONCLUSIONS

In summary, we have theoretically and numerically investigated the trapping effect and the optical performances of SPPs on the graphene-based graded grating structure. We find that the SPPs at different frequencies within a broadband region can be slowed down and trapped at different positions in the graphene surface. The applied gate voltages can be employed to efficiently tune the trapping positions and group velocities of the trapped SPPs. Thus, inputting optical signals with different frequencies can be accordingly separated and trapped at different positions in the graphene surface, which can be used as a broadband spectrometer. Also, the release mechanism is discussed in terms of real-time modification of the gate voltage. Once a certain threshold voltage for a given trapped wave is reached, the wave will finally be out of the graded grating zone. The trapped waves within a broad frequency band are predicted to propagate along the graphene or out of the graded grating zone by modulating the dispersion curve via bias voltage. In a word, the unique optical features of the graphene-based graded grating structure can be applied in the novel designs of the plasmonic devices targeted toward the applications in optical buffers, spectrometer, optical switching, slow-light systems, and nonlinear optical devices.

**Funding.** Fundamental Research Funds for the Central Universities (JD2017JGPY0005); National Natural Science Foundation of China (NSFC) (61775050).

**Acknowledgment.** The authors gratefully acknowledge the financial support for this work from the National Natural Science Foundation of China and the Fundamental Research Funds for the Central Universities.

## REFERENCES

1. E. Ozbay, "Plasmonics: merging photonics and electronics at nanoscale dimensions," Science **311**, 189–193 (2006).
2. D. Gacemi, J. Mangeney, R. Colombelli, and A. Degiron, "Subwavelength metallic waveguides as a tool for extreme confinement of THz surface waves," Sci. Rep. **3**, 1369 (2013).
3. B. Guo, W. Shi, and J. Yao, "Slowing and trapping THz waves system based on plasmonic graded period grating," J. Opt. **45**, 50–57 (2016).
4. R. Gordon, A. G. Brolo, D. Sinton, and K. L. Kavanagh, "Resonant optical transmission through hole-arrays in metal films: physics and applications," Laser Photon. Rev. **4**, 311–335 (2010).
5. F. H. Koppens, D. E. Chang, and F. J. Garcia de Abajo, "Graphene plasmonics: a platform for strong light-matter interactions," Nano Lett. **11**, 3370–3377 (2011).
6. A. Vakil and N. Engheta, "Transformation optics using graphene," Science **332**, 1291–1294 (2011).
7. H. J. Xu, W. B. Lu, Y. Jiang, and Z. G. Dong, "Beam-scanning planar lens based on graphene," Appl. Phys. Lett. **100**, 051903 (2012).
8. T. Zhang, L. Chen, and X. Li, "Graphene-based tunable broadband hyperlens for far-field subdiffraction imaging at mid-infrared frequencies," Opt. Express **21**, 20888–20899 (2013).
9. C. H. Gan, H. S. Chu, and E. P. Li, "Synthesis of highly confined surface plasmon modes with doped graphene sheets in the midinfrared and terahertz frequencies," Phys. Rev. B **85**, 125431 (2012).
10. L. Chen, T. Zhang, X. Li, and G. Wang, "Plasmonic rainbow trapping by a graphene monolayer on a dielectric layer with a silicon grating substrate," Opt. Express **21**, 28628–28637 (2013).
11. H. Lu, C. Zeng, Q. Zhang, X. Liu, M. M. Hossain, P. Reineck, and M. Gu, "Graphene-based active slow surface plasmon polaritons," Sci. Rep. **5**, 8443 (2015).
12. H. Nasari and M. S. Abrishamian, "Nonlinear manipulation of surface plasmon polaritons in graphene based bragg reflector," J. Lightwave Technol. **33**, 4071–4078 (2015).
13. B. Shi, W. Cai, X. Zhang, Y. Xiang, Y. Zhan, J. Geng, M. Ren, and J. Xu, "Tunable band-stop filters for graphene plasmonics based on periodically modulated graphene," Sci. Rep. **6**, 26796 (2016).

14. M. Yarahmadi, M. K. Moravvej-Farshi, and L. Yousefi, "Subwavelength graphene-based plasmonic THz switches and logic gates," IEEE Trans. Terahertz Sci. Technol. **5**, 725–731 (2015).
15. R. Hao, J. Jin, X. Peng, and E. Li, "Dynamic control of wideband slow wave in graphene based waveguides," Opt. Lett. **39**, 3094–3097 (2014).
16. J. Christensen, A. Manjavacas, S. Thongrattanasiri, F. H. Koppens, and F. J. García de Abajo, "Graphene plasmon waveguiding and hybridization in individual and paired nanoribbons," ACS Nano **6**, 431–440 (2011).
17. Z. Fei, A. S. Rodin, G. O. Andreev, W. Bao, A. S. McLeod, M. Wagner, L. M. Zhang, Z. Zhao, M. Thiemens, G. Dominguez, M. M. Fogler, A. H. Gastro Neto, C. N. Lau, F. Keilmann, and D. N. Basov, "Gate-tuning of graphene plasmons revealed by infrared nano-imaging," Nature **487**, 82–85 (2012).
18. K. S. Novoselov, A. K. Geim, S. V. Morozov, D. Jiang, Y. Zhang, S. V. Dubonos, I. V. Grigorieva, and A. A. Firsov, "Electric field effect in atomically thin carbon films," Science **306**, 666–669 (2004).
19. B. Wang, X. Zhang, F. J. García-Vidal, X. Yuan, and J. Teng, "Strong coupling of surface plasmon polaritons in monolayer graphene sheet arrays," Phys. Rev. Lett. **109**, 073901 (2012).
20. M. Jablan, H. Buljan, and M. Soljačić, "Plasmonics in graphene at infrared frequencies," Phys. Rev. B **80**, 245435 (2009).
21. J. Lott, C. Xia, L. Kosnosky, C. Weder, and J. Shan, "Terahertz photonic crystals based on barium titanate/polymer nanocomposites," Adv. Mater. **20**, 3649–3653 (2008).
22. L. Chen, G. P. Wang, Q. Gan, and F. J. Bartoli, "Trapping of surface-plasmon polaritons in a graded Bragg structure: frequency-dependent spatially separated localization of the visible spectrum modes," Phys. Rev. B **80**, 161106 (2009).
23. T. F. Krauss, "Slow light in photonic crystal waveguides," J. Phys. D **40**, 2666–2670 (2007).
24. Q. Gan and F. J. Bartoli, "Surface dispersion engineering of planar plasmonic chirped grating for complete visible rainbow trapping," Appl. Phys. Lett. **98**, 251103 (2011).
25. Q. Gan, Y. J. Ding, and F. J. Bartoli, ""Rainbow" trapping and releasing at telecommunication wavelengths," Phys. Rev. Lett. **102**, 056801 (2009).
26. Q. M. Zhang, H. Li, M. Poh, F. Xia, Z. Y. Cheng, H. Xu, and C. Huang, "An all-organic composite actuator material with a high dielectric constant," Nature **419**, 284–287 (2002).
27. J. Li, J. He, and Z. Hong, "Terahertz wave switch based on silicon photonic crystals," Appl. Opt. **46**, 5034–5037 (2007).
28. F. Zangeneh-Nejad, S. AbdollahRamezani, K. Arik, and A. Khavasi, "Beam focusing using two-dimensional graphene-based meta-reflect-array," in *24th Iranian Conference on Electrical Engineering (ICEE)* (IEEE, 2016), pp. 613–616.
29. J. S. Gómez-Díaz and J. Perruisseau-Carrier, "Graphene-based plasmonic switches at near infrared frequencies," Opt. Express **21**, 15490–15504 (2013).
30. K. S. Novoselov, A. K. Geim, S. V. Morozov, D. Jiang, M. I. Katsnelson, I. V. Grigorieva, S. V. Dubonos, and A. A. Firsov, "Two-dimensional gas of massless Dirac fermions in graphene," Nature **438**, 197–200 (2005).
31. Y. J. Lu, J. Kim, H. Y. Chen, C. Wu, N. Dabidian, C. E. Sanders, C.-Y. Wang, M.-Y. Lu, B.-H. Li, X. Qiu, W.-H. Chang, L.-J. Chen, G. Shvets, C.-K. Shih, and S. Gwo, "Plasmonic nanolaser using epitaxially grown silver film," Science **337**, 450–453 (2012).